

# Seeking Spinning Subpopulations of Black Hole Binaries via Iterative Density Estimation

Jam Sadiq<sup>1, 2, \*</sup>, Thomas Dent<sup>3</sup>, and Ana Lorenzo-Medina<sup>3</sup>

<sup>1</sup> SISSA, Via Bonomea 265, 34136 Trieste, Italy and INFN Sezione di Trieste

<sup>2</sup> IFPU - Institute for Fundamental Physics of the Universe, Via Beirut 2, 34014 Trieste, Italy and

<sup>3</sup> IGFAE, University of Santiago de Compostela, E-15782 Spain

(Dated: June 8, 2025)

Attempts to understand the formation of binary black hole (BBH) systems detected via gravitational wave (GW) emission are affected by many unknowns and uncertainties, from both the observational and theoretical (astrophysical modelling) sides. Binary component spins have been proposed as a means to investigate formation channels, however obtaining clear inferences is challenging, given the apparently low magnitude of almost all merging BH spins and their high measurement uncertainties. Even for the effective aligned spin  $\chi_{\text{eff}}$  which is more precisely measured than component spins, specific model assumptions have been required to identify any clear trends. Here, we reconstruct the joint component mass and  $\chi_{\text{eff}}$  distribution of BBH mergers with minimal assumptions using the GWTC-3 catalog, using an iterative kernel density estimation (KDE)-based method. We reproduce some features seen in previous analyses, for instance a small but preferentially positive  $\chi_{\text{eff}}$  for low-mass mergers; we also identify a possible subpopulation of higher-spin BBH with  $|\chi_{\text{eff}}|$  up to  $\sim 0.75$  for primary masses  $m_1 \gtrsim 40 M_{\odot}$ , in addition to the bulk of the distribution with  $|\chi_{\text{eff}}| \lesssim 0.2$ . This finding is consistent with previous studies indicating a broader spin distribution at high mass, suggesting a distinct origin for the high-spin systems. We also identify a previously-unnoticed trend at lower masses: the population mean of  $\chi_{\text{eff}}$  increases (decreases) with  $m_1$  ( $m_2$ ) within the overdensity around  $m_1 \sim 10 M_{\odot}$ . This “spin fine structure” may partly explain a previously reported anticorrelation between mass ratio and  $\chi_{\text{eff}}$ .

## I. INTRODUCTION

Ever since the first gravitational wave (GW) detection revealed a binary black hole (BBH) source with the—previously unsuspected—component masses of around  $35 M_{\odot}$  [1, 2], LIGO-Virgo observations [3, 4] of compact binaries have continued to yield surprises. Having a set of detected compact binaries, such as the order(100) candidates catalogued in the GWTC releases [5–8], it is possible to study population properties of these compact binaries and eventually draw implications from these properties on binary astrophysical formation and evolution [9, 10].

Black hole spins have been proposed as a key diagnostic in understanding binary formation channels [11–14], though presenting persistent challenges in interpretation: recent studies towards this include [15–22]. In isolated binaries, spins are expected to exhibit a preferred alignment with the orbital axis, breaking symmetry between prograde and retrograde configurations—assuming that magnitudes are not negligible [though see 23]. In contrast, dynamically formed binaries in clusters should have randomized spin orientations, restoring approximate symmetry between aligned and in-plane spins (with possible exceptions, e.g. triple systems, post-encounter tidal locking and AGN environments). Hierarchical mergers introduce distinct signatures: remnants from near-equal-mass mergers tend to have dimensionless spin magnitudes  $|\vec{s}| \sim 0.7$ , and if retained in dense envi-

ronments their orientations in subsequent mergers should again randomize.

However, observational limitations severely complicate such tests and signatures. Current gravitational-wave observations alone are insufficient to draw definite conclusions about BBH formation channels or environments. Most black hole spins are small or consistent with zero, in-plane components are largely unmeasurable for binary black holes, and even aligned spins often suffer from large uncertainties (which are correlated with binary mass ratio  $q \equiv m_2/m_1$  [24–26]). On the astrophysics side, the likelihood that multiple formation channels are contributing to the observed population [16, 27] implies that first, inferences on the spin properties of detected BBH *as a whole* are probably not a good representation of any one channel. Therefore, direct interpretation of the inferred spin distribution without allowing for multiple subpopulations [27] is likely misleading. Secondly, as different channels may well be (partly or completely) separated over various dimensions of the BBH parameter space, i.e. component mass and possibly redshift [see e.g. 28, 29], it will be critical to allow for *correlations between spins and other BBH parameters*, including a possible mixture of *subpopulations* which may mimic correlated trends.

Given this complexity, the utility of spins remains limited: to make progress on the observational side, significant improvements in measurement precision (implying higher S/N) and a much greater sample size may be needed, and on the modelling side, more detailed and realistic scenarios encompassing multiple channels. To guide such efforts, it is crucial to make full use of cur-

\* Corresponding email: jamlucky.qau@gmail.com

rently available observations, including evidence for correlations or subpopulations: by refining empirical constraints on mass, spin, and redshift distributions, we can lay the groundwork for future studies to test formation models as the catalog grows.

Currently, some features in the BBH joint spin/mass/redshift distribution have been identified under various more or less restrictive model assumptions, and proposed as pointers towards formation channels. These assumptions or methods may be divided into parameterized models, where Bayesian hierarchical inference is used to determine posteriors for a small number of hyper-parameters corresponding to a relatively simple distribution function [e.g. 30, 31]; and semi- or non-parametric models, which aim to learn population properties from the data, either without requiring any specific functional form, or (for semi-parametric models) allowing for generalised deviations from a given parametric model [32–43]. Without attempting a complete summary of these findings, we can identify critical aspects of possible correlations between BH spins and other population properties.

As mentioned earlier, many studies consider primarily the effective orbit-aligned spin  $\chi_{\text{eff}} \equiv (s_{1z} + qs_{2z})/(1+q)$ , which is more precisely measured than other spin variables [44] and so is often considered as a proxy for spin magnitude (though its sign is also informative on alignment). [35] found via a flexible Gaussian mixture model that the magnitude  $|s_z|$  (assumed identically distributed over binary components) has a wider distribution for chirp mass  $\mathcal{M} \equiv (m_1 m_2)^{3/5}/(m_1 + m_2)^{1/5} \gtrsim 35 M_\odot$ . [45] found an apparently significant negative correlation of  $\chi_{\text{eff}}$  with  $q$ , though without attempting to identify its origin in BBH subpopulations or formation channels. [29, 46] determined that the  $\chi_{\text{eff}}$  distribution of widens at higher redshift, though such a trend is hard to distinguish from a correlation with mass given the strong selection effects that relate mass and distance [47, 48].

More recently, efforts have been made to identify specific subpopulations with different spin properties [e.g. 49, 50]. [51] tailored a non-parametric mixture model taking as a reference the global peak of the local BBH merger distribution, with component masses  $\sim 10 M_\odot$  and small positive  $\chi_{\text{eff}}$ , finding mild evidence for a high-mass ( $m_1 \gtrsim 50 M_\odot$ ) subpopulation with a broader  $\chi_{\text{eff}}$  distribution symmetric about zero. By contrast, [52] found with a binned non-parametric analysis that the  $30 - 40 M_\odot$  component mass range containing the bulk of detections has a distinct  $\chi_{\text{eff}}$  distribution symmetric about 0, suggesting a possible globular cluster origin [53], while the remainder of the population tends to positive  $\langle \chi_{\text{eff}} \rangle$ . Recently, [22] designed a change-point analysis to find a transition between a narrow, positive  $\chi_{\text{eff}}$  distribution below, vs. a broad, uniform and symmetric  $\chi_{\text{eff}}$  distribution above, a critical mass determined to be  $\simeq 45 M_\odot$ , interpreting the higher-mass population as due to hierarchical formation in dense clusters. Such an interpretation would be consistent with 1st generation

BH (those formed from stellar collapse) having low spins and masses limited by pair-instability supernova (PISN) dynamics [for which see e.g. 28, 68].

Investigations using parametrized models of spin magnitude observables  $|s_{1,2}|$  have yielded comparable findings of a high-mass subpopulation with larger spins [54–56], though the higher number of degrees of freedom, including tilt angles, in this case may mean that detailed population properties are more affected by potential mis-modeling bias.

The lack of unanimity in findings when analyzing the same (GWTC-3 [8]) data set reflects the high uncertainties in spin measurements (even if considering  $\chi_{\text{eff}}$ ): due to these uncertainties the choice of model assumptions can strongly affect inferences on the spin distribution, and thus also the interpretation of individual events. For parameterized models, it is generally not possible to quantify biases due to the model differing from the true population (mis-modelling) beyond self-consistency checks which, for data with large uncertainties, provide weak constraints. Even for non-parametric methods, any assumption that the population distribution factorizes over different parameters (implying a lack of correlations) could lead to significant biases. In particular, due to correlated measurement uncertainties in  $\chi_{\text{eff}}$  and  $q$ , any assumption that the BBH mass, or mass ratio distribution takes a specific form may induce biases in spin inference (and vice versa).

Therefore, to obtain an estimate of the joint spin-mass distribution we are led to consider, at a minimum, a fully three-dimensional non-parametric framework allowing for correlations between both BBH component masses and  $\chi_{\text{eff}}$ . So far this approach was only taken by [52] using a binned (stepwise constant) model, where some correlations or features may be obscured by the (relatively large) bin size, and without reporting the full mass-spin distribution. We demonstrated the technical feasibility of a 3d population reconstruction using a flexible adaptive KDE [37, 40] in [43], where the “resolution” of the population estimate (i.e. how rapidly it may vary over BBH parameter space) is regulated by the local event density.<sup>1</sup>

In this work we then apply the same fully non-parametric, i.e. data-determined, method to reconstruct the BBH spin-mass distribution. The remainder of the paper is organized as follows: in section 2 we motivate and explain the method in outline, highlighting aspects where the application to effective spins differs from previous cases. In section 3 we apply our method to detected BBH in GWTC-3 using the available LIGO-Virgo-KAGRA (LVK) parameter estimation (PE) [58]; we compare the resulting mass distribution with our previous

<sup>1</sup> [57], using a general finely-binned 2-d non-parametric method to investigate correlations, is the closest to us in approach and finds partly comparable results while restricted to the 2-d space of primary mass and  $\chi_{\text{eff}}$ .

studies [40] and assess the evidence for possible spin correlations or subpopulations. In section 4 we discuss the implications of our results and consider possible further investigations.

## II. METHOD

### A. Summary of multidimensional iterative adaptive KDE

For our non-parametric population reconstruction, we employ a recently developed generalized iterative KDE method [43] which extends our previous work [37, 40] using previous versions of the method to investigate the LVK detected catalog, and also to demonstrate population estimation for “light seed” BH in mock LISA data [59]. The key development in the most recent version is to replace spherical (isotropic) kernels by elliptical or ellipsoidal, in other words allowing for independent choice or optimization of bandwidth along different dimensions of parameter space. Rather than repeat the exposition of the complete method in [43], here, after explaining the general expression for the adaptive KDE of a given set of observations (events)  $\vec{X}_i$ ,  $i = 1 \dots N$ , we set out briefly how our application of the KDE addresses the fundamental statistical issues in population reconstruction for GW events, and summarize the expected strengths and weaknesses of the method.

The estimated probability density  $\hat{f}(\vec{x})$  at point  $\vec{x}$  from a multidimensional Gaussian adaptive KDE is given by

$$\hat{f}(\vec{x}) = \frac{1}{N \sqrt{(2\pi)^D |\Sigma|}} \sum_{i=1}^N \frac{1}{\lambda_i} \exp \left( -\frac{1}{2} (\vec{x} - \vec{X}_i)^T \lambda_i^{-2} \Sigma^{-1} (\vec{x} - \vec{X}_i) \right) \quad (1)$$

where  $D$  is the dimensionality of the data,  $\Sigma$  is the global kernel covariance matrix (which we take to be the same for all data points), and the local adaptive parameter  $\lambda_i$  is given by:

$$\lambda_i = \left( \frac{\hat{f}_0(\vec{X}_i)}{g} \right)^{-\alpha}, \quad \log g = N^{-1} \sum_{i=1}^N \log \hat{f}_0(\vec{X}_i). \quad (2)$$

Here  $\hat{f}_0$  is an initial pilot density estimate obtained by setting  $\lambda_i = 1$ ,  $\alpha$  is the bandwidth sensitivity parameter (lying between 0 and 1), and  $g$  is a normalization factor ensuring that the product of  $\lambda_i$  over all events is unity. Our previous implementations were constrained by spherical kernels in standardized coordinates ( $\Sigma = h^2 \mathbb{I}$ , where  $\mathbb{I}$  is the identity matrix), however in [43] we added flexibility by allowing per-dimension bandwidths as  $\Sigma = \text{diag}(h_1^{-2}, h_2^{-2}, \dots)$ . In principle a more general off-diagonal kernel matrix can be chosen, however our approach is intended to limit complexity and avoid the possibility that off-diagonal kernels might artificially enhance apparent correlations between parameters.

### 1. Bias-variance tradeoff: Bandwidth selection

It is well known that bandwidth selection is crucial to control KDE errors and uncertainties [e.g. 60], with too large bandwidth leading to a “smooth” but biased estimate which understates density variations, and conversely too small bandwidth leading to over-fitting with spuriously large fluctuations in the estimate and excessive variance over realizations. Bandwidth choice is strongly linked to the finite statistics of detected events, since smaller bandwidth (in standardized coordinates) is appropriate for larger  $N$ . We choose the multi-dimensional bandwidth  $\vec{h} \equiv (h_1, h_2 \dots)^T$  by maximizing the expected likelihood of the data set, evaluated by ( $k$ -fold) cross-validation (technically, the sum of log likelihoods over the  $k$  folds).<sup>2</sup> The same optimization determines the adaptive parameter  $\alpha$ , which controls the scaling of the local bandwidth with the (pilot) density at the data points. Adaptive KDE is crucial to obtaining a stable estimate with low bias given that the density of observations varies by orders of magnitude across the BBH parameter space [37].

### 2. Uncertainty due to finite event statistics

Given the relatively small number of GW observations, any estimate of the population distribution has a non-trivial uncertainty, characterized by considering the observed events as an inhomogeneous Poisson process. We estimate this uncertainty by analyzing several hundred bootstrap resampled data sets, constructed by taking Poisson(1) samples corresponding to each observed BBH. We then take the median, symmetric 90% intervals, etc., over some set of bootstrap resampled KDE outputs.

### 3. Selection Function

The strategy described so far can naturally be applied to detected GW events, however these are a strongly biased sample of all mergers, even if we consider only the local Universe. More massive BBH events produce (up to some limit) significantly higher S/N than lower mass, and at constant mass higher  $\chi_{\text{eff}}$  gives higher S/N [26, 44]. For our study, where any evolution over redshift is neglected (given the narrow range of  $z$  currently accessible for the bulk of the BBH population [43]), we quantify selection by the sensitive volume-time (VT) which relates the detected number density of events to the astrophysi-

<sup>2</sup> Note that the distribution that maximizes the likelihood of the data  $\vec{X}_i$  is a sum of delta functions [61], comparable to the low-bandwidth limit of KDE which tends to infinite variance.

cal merger rate density  $\mathcal{R}$  as

$$dN_{\text{det}}(m_1, m_2, \chi_{\text{eff}}) = \text{VT}(m_1, m_2, \chi_{\text{eff}}) d\mathcal{R}(m_1, m_2, \chi_{\text{eff}}). \quad (3)$$

We use an accurate fit to the probability of detection of simulated BBH signals in O3 data from [48], using publicly released LVK analysis results [62, 63];<sup>3</sup> we further integrate over luminosity distance, assuming a rate uniform in comoving volume-time, to compute VT at each point.

#### 4. Parameter measurement uncertainty

In addition to the above effects, the properties of each event are uncertain due to detector noise, with most BBH having low S/N of order(10). This uncertainty is quantified by providing “PE” samples, which represent the multi-dimensional Bayesian posterior density for each significant detected event [8, 58, 64]. The standard posterior calculation uses an assumed uninformative prior probability over BH masses and spins: more specifically, a uniform distribution over redshifted apparent (“detector frame”) component masses and over spin magnitudes  $|\vec{s}_{1,2}|$ , and a isotropic distribution over spin directions. As discussed in [e.g. 30, 31], the posteriors are only optimal and unbiased if the actual population distribution is equal to the prior. In general, we will obtain more accurate parameter estimates by replacing the “PE” mass and spin prior by an estimate of the astrophysical population distribution.

We implement this technically by *iterative* density estimation with reweighting of the posterior samples [40]. To begin, we randomly select 100 posterior samples for each event using weights proportional to the *inverse* PE prior over  $\chi_{\text{eff}}$ , given the sample’s component masses [65]. This reweighted parameter sample set corresponds to a *uniform* prior over  $\chi_{\text{eff}}$ . Then, at each iteration, we evaluate a pre-existing KDE of the detected population distribution at each sample point and obtain an astrophysical distribution estimate  $f_{\text{pop}}$  by dividing by  $\text{VT}(m_1, m_2, \chi_{\text{eff}})$ .

We then select Poisson(1) samples for each event, not with uniform random sampling but weighted by these relative merger densities, divided by the PE prior over masses, which is uniform except for the  $(1+z)$  factor relating source to apparent “detector frame” masses.<sup>4</sup> This bootstrapped reweighted sample set is then used to generate the next KDE iteration.

We thus build up a Markov chain of population density estimates: if this reaches an approximately stationary

state, it will represent a self-consistent Monte Carlo estimate of the population distribution and the parameters of each event, including the uncertainties of both [40]. We monitor the approach to stationarity by examining time series of the optimized bandwidth and adaptive parameters over iterations, and calculating their autocorrelations. Typically the autocorrelations appear negligible after order(100) iterations [40], thus we discard the first few  $\times 100$  evaluations and use the remaining KDEs to generate final results.<sup>5</sup>

#### B. Tests and expected biases of iterative KDE reconstruction

Simple 1d and 2d mock data tests of iterative KDE reconstruction, showing that it can properly account for PE uncertainty, have been presented in [40], and a detailed end-to-end mock data test on LISA “light seed” BBH sources was carried on in [59], demonstrating its performance in the case of strongly correlated errors in the source total mass and redshift. However, the iterative KDE has some inherent limitations in its ability to represent and reconstruct the true population, which should be understood before interpreting our results.

##### 1. Parameter resolution and scale of density variations

The most obvious restriction is that the Gaussian KDE cannot represent abrupt, step-function-like variations in density over the source parameter space (see [40] for a mock data example). The impact of this restriction to a “smooth” functional form also varies with the local density of detected events, due to the adaptive kernel choice Eq. (2): the (log of the) estimated density may vary rapidly in regions with a high number of detections, but must be slowly varying in sparsely populated regions. While this is desirable to prevent over-fitting and excess variance, it limits the possible parameter dependence of the estimated population. In particular, if the true population does contain abrupt steps or very narrow peak features, we expect the KDE to provide an “over-smoothed” reconstruction, and also that the amount of excess smoothing will decrease (i.e., the resolution of the estimate will improve) with higher numbers of detected events.

##### 2. Behavior in regions with low event count

A related but distinct limitation concerns the limit of the KDE in regions far from most detected events,

<sup>3</sup> These and other publicly released GWTC-3 data sets can be accessed at <https://gwosc.org/GWTC-3/>.

<sup>4</sup> We sample *without* replacement, to avoid the case that copies of the same PE sample are included in both the training and test sets during  $k$ -fold likelihood evaluation, which would bias towards small bandwidth.

<sup>5</sup> In more detail, for our results we generate the pre-existing distribution estimate used for  $f_{\text{pop}}$  in sample reweighting as a mean over a buffer of the previous 100 iterations.

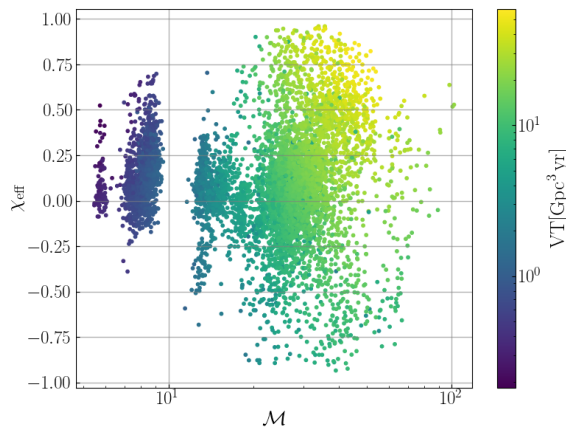


FIG. 1. Chirp mass  $\mathcal{M}$  and  $\chi_{\text{eff}}$  of PE samples for 69 BBH events from GWTC-3, reweighted to a uniform  $\chi_{\text{eff}}$  prior, with colors showing the sensitive volume-time (VT).

where a small number of kernels (possibly only a single kernel) contribute non-negligibly. Here the estimate for the distribution of detected events must go towards zero with a Gaussian dependence, and will be dominated at large distance by the kernel with highest bandwidth. The consequences for the astrophysical population estimate will depend on the dependence of the selection function.<sup>6</sup> Considering the space of binary masses and spins, the selection function VT typically varies as a power law or polynomial [47, 48], thus the estimated astrophysical distribution far from the detected signal points will also be dominated by the Gaussian falloff of the “broadest kernel”. Of course, the uncertainties in rate density for such points where only order(1) detected events contribute will be extremely large (typically orders of magnitude), as reflected in the bootstrap estimates.

### III. APPLICATION TO GWTC-3 DATA

We apply the iterative reweighted KDE to GWTC-3 public data [58], selecting 69 BBH candidate events from the cumulative O1-O3 catalog which have a false alarm rate below 1 per year and excluding GW190814, an outlier event with an unusually low secondary mass ( $m_2 \simeq 2.6 M_\odot$ ) [66], as this system could represent either a very massive neutron star or a light black hole, which is inconsistent with the primary BBH population we aim to analyze. As stated above we draw 100 random samples from the posterior for each BBH event, reweighted to a uniform prior in effective spin  $\chi_{\text{eff}}$ . The sensitive VT estimates from [48] at the masses and  $\chi_{\text{eff}}$  of the samples are shown in Fig. 1.

<sup>6</sup> See [43, 59] for a more detailed discussion of the selection function dependence on mass and distance.

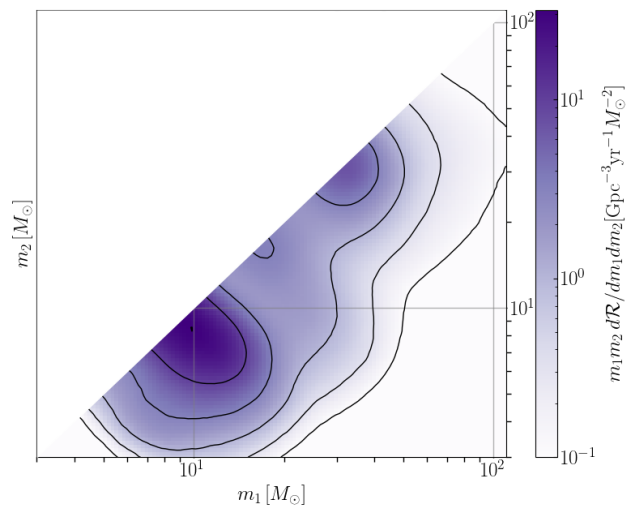


FIG. 2. Merger rate density over binary component masses, marginalized over  $\chi_{\text{eff}}$ . Median estimate over bootstrap iterations.

We perform KDEs over the logarithms of source component masses  $\ln m_1$ ,  $\ln m_2$ , and  $\chi_{\text{eff}}$ , ensuring proper exchange symmetry by “reflecting” each  $(\ln m_1, \ln m_2)$  sample point, i.e. also including the mass-exchanged point  $(\ln m'_1 = \ln m_2, \ln m'_2 = \ln m_1)$  in the KDE data [40]. Having obtained some hundreds of bootstrap estimates of the detected distribution, we evaluate these estimates on a 3d grid for visualization, and convert to astrophysical merger rate density by multiplying by the total number of detected events and dividing by VT evaluated on the same 3d grid.

#### A. Marginalized mass distributions

From the 3d rate estimates, we first marginalize over the  $\chi_{\text{eff}}$  dimension to obtain the merger rate as a function of the binary component masses. The resulting two-dimensional mass distribution in Fig. 2 is similar to that found under the assumptions previously made in [40], which neglected spin in selection effects and effectively assumed the population  $\chi_{\text{eff}}$  distribution to be equal to the PE prior (i.e. symmetric around zero). In particular, the primary and secondary masses appear anti-correlated in the neighborhood of the  $\sim 10 M_\odot$  peak, with significant support for unequal mass binaries: i.e., contours of constant rate density are approximate ellipses with major axis parallel to a line  $m_1 m_2 = \text{const.}$ . Conversely, the  $\sim 30 M_\odot$  peak is concentrated near the equal mass line, and the secondary mass distribution declines rapidly above  $\sim 35 M_\odot$ . We observe minor differences in the high-mass regime. Additionally, overall rates are somewhat lower than those estimated under the zero-spin assumption, possibly reflecting the influence of aligned spin on the detection probability (and thus on VT).

We further marginalize over each component mass

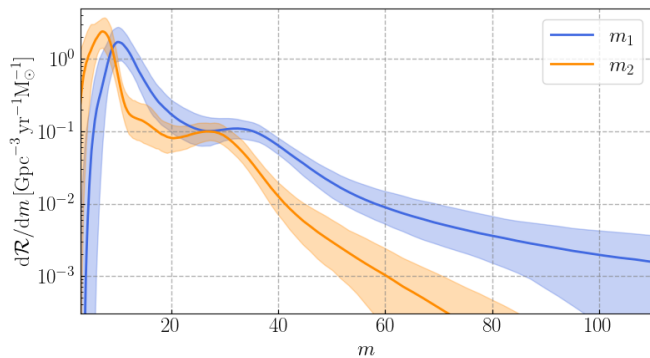


FIG. 3. Rate density over BBH component masses obtained by marginalizing 3d rate estimates over  $\chi_{\text{eff}}$  and one component mass. Color bands show 90% confidence regions obtained from bootstrap iterations.

component to obtain one-dimensional merger rates over primary and secondary masses, shown in Fig. 3. The resulting 1d rates are again consistent with our previous analysis neglecting the population  $\chi_{\text{eff}}$  distribution, but again with minor overall shifts in the estimated rates which likely reflect the inclusion of aligned spin dependence in VT.

### B. Dependence of aligned spin on binary masses

Although it is impossible in practice to visualize the full 3d mass-spin distribution with uncertainties, we start by characterizing the dependence of basic statistical properties of the population  $\chi_{\text{eff}}$  distribution as functions of  $(m_1, m_2)$ . We show the *population mean*  $\chi_{\text{eff}}$  (median estimate over bootstrap iterations) over the 2d mass plane in Fig. 4. We see a number of interesting features: the local maximum of merger rate near  $m_1 = m_2 = 30 M_\odot$  has small but marginally positive  $\langle \chi_{\text{eff}} \rangle$ , while the region around  $m_1 \simeq m_2 \simeq 20 M_\odot$  has zero population mean. Conversely, the distribution at lower secondary mass shows an apparent trend towards higher  $\langle \chi_{\text{eff}} \rangle$  at unequal mass, reflecting the correlation found in [45]. At high masses and far from the detected events the population trends towards negative  $\langle \chi_{\text{eff}} \rangle$ , which may primarily reflect random variation in regions with small number statistics.

We further show the *population standard deviation* of  $\chi_{\text{eff}}$  in Fig. 5, as a measure of the spread of the spin distribution. This measure remains small over most of the parameter space except for primary mass above  $\sim 40 M_\odot$  and secondary above  $\sim 25 M_\odot$ , where we observe a rapid increase in  $\sigma(\chi_{\text{eff}})$ . (The standard deviation also becomes large far from the detected events, where small number statistics dominate.) An increase in the width of the  $\chi_{\text{eff}}$  distribution at higher masses was proposed in [22, 67] as a potential signature of hierarchical BBH formation, if 1st generation BH are assumed to have masses limited

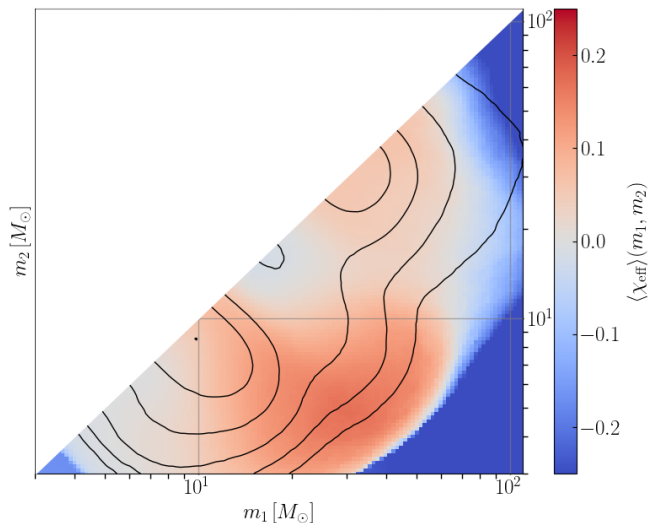


FIG. 4. Population mean  $\chi_{\text{eff}}$  as a function of BH component masses (median estimate over bootstrap iterations). Contours show rate density as in Fig. 2.

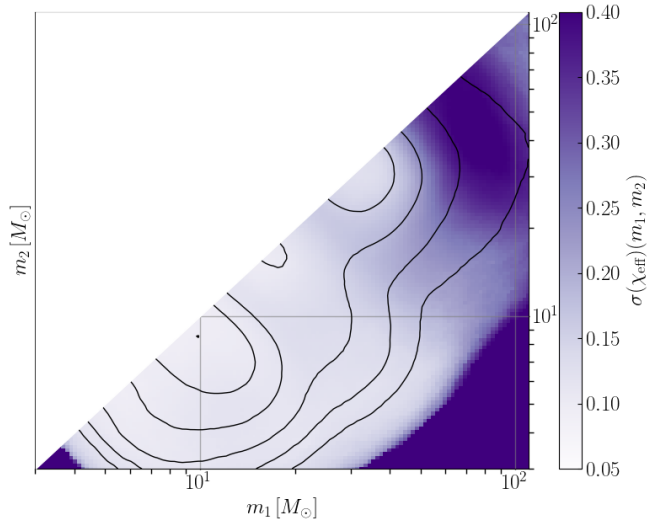


FIG. 5. Population standard deviation of  $\chi_{\text{eff}}$  as a function of BH component masses (median estimate over bootstrap iterations). Contours show rate density as in Fig. 2.

by PISN dynamics and to have small spin magnitudes, and given that 2nd generation BH have spin magnitudes of order 0.7. We observe a relatively sharp transition to a broad spin distribution above  $m_1 \simeq 40 M_\odot$ ; the coincidence of this approximate mass scale with stellar evolution estimates of the PISN “gap” was noted in [22] as further motivating dynamic and hierarchical formation for heavier BH in merging binaries.



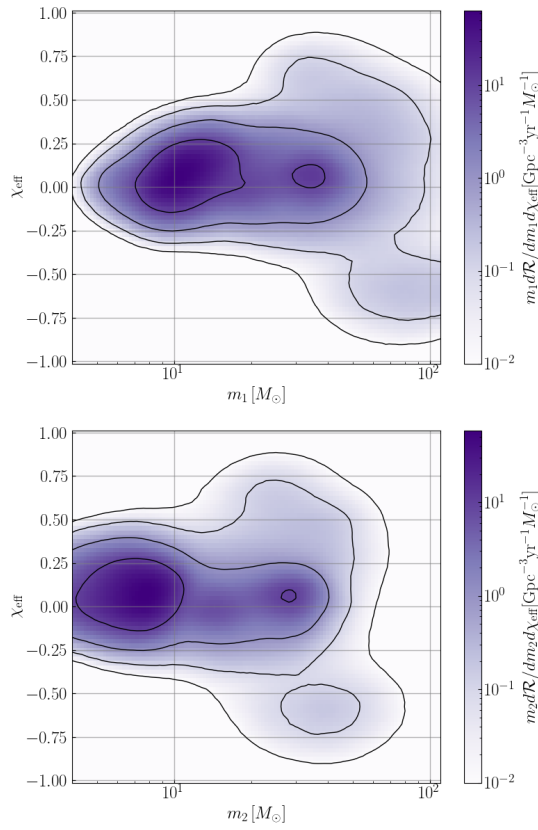


FIG. 6. 2d rate density over binary component mass and  $\chi_{\text{eff}}$  (median estimate over bootstrap iterations). Left: marginalized over  $m_2$ ; right, marginalized over  $m_1$ .

### C. Mass and effective spin

We may isolate trends over primary or secondary mass by plotting the  $\chi_{\text{eff}}$  distribution directly, marginalizing over the other component mass, as shown in Figure 6. We see a strong concentration of events at low to intermediate masses ( $\sim 10 M_{\odot} - \sim 35 M_{\odot}$ ) and near-zero effective spin (slightly positive for the  $\sim 10 M_{\odot}$  peak), consistent with previous findings [52, 57]. However, we also observe nontrivial additional structure at higher masses ( $m_1 > 30 M_{\odot}$ ,  $m_2 > 20 M_{\odot}$ ) with a larger spread of non-zero spin values. The peaks near  $\chi_{\text{eff}} = 0$  appear to co-exist with this broader sub-population over some range of mass. The significance of these trends can be visualized by selecting discrete values of the component masses and computing the normalized distribution of  $\chi_{\text{eff}}$  for each, as in Fig. 7. We indeed see an increase in the spread of the  $\chi_{\text{eff}}$  distribution as  $m_1$  increases from  $35 M_{\odot}$  through  $55 M_{\odot}$ , although statistical uncertainties dominate at  $65 M_{\odot}$  (and higher masses which we do not plot). Significant trends over  $m_2$  are, though, harder to identify; this difference may be expected as the secondary BH makes a smaller contribution to  $\chi_{\text{eff}}$  simply by construction.

The low-mass region also shows interesting structure:

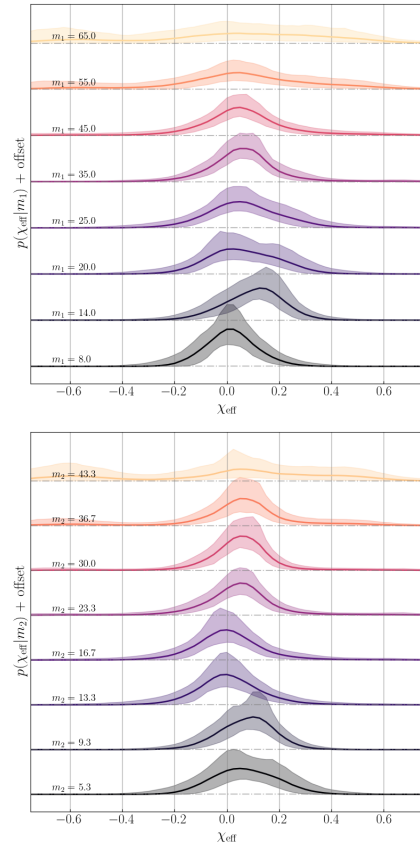


FIG. 7. Normalized merger rate distributions over effective spin at constant component mass. Top: Population distribution of  $\chi_{\text{eff}}$  marginalizing over  $m_2$  at constant  $m_1$  values. Bottom: Distribution of  $\chi_{\text{eff}}$  marginalizing over  $m_1$  at constant  $m_2$ . We show the median and symmetric 90% confidence intervals over bootstrap iterations and apply constant vertical offsets for visual clarity.

the mean of  $\chi_{\text{eff}}$  shifts from near zero at the lowest masses to clearly positive at  $m_1 \sim 14 M_{\odot}$ , then closer to zero at  $m_1 \sim 20 M_{\odot}$  and above, a trend also visible in Fig. 4. It is believed that the low-mass peak is associated with isolated binary formation [51, 53], for which mass transfer effects (either stable or common-envelope) may play important roles in determining BH spins [e.g. 69, 70]; stable mass transfer [71] has been discussed as a possible origin for correlations between binary mass ratio and aligned spin [18, 21]. Alternatively, more complex scenarios where different sub-populations coexist even at low mass may be responsible for such trends [72]. While our findings do not match any specific model, the ability of our 3d analysis to localize mass-spin correlations in parameter space may provide a crucial guide to identify the relevant effects.

Lastly, we further investigate the significance of variations in  $\chi_{\text{eff}}$  by plotting the dependence of its population statistics (mean and standard deviation) against component masses, as in Fig. 8. The population mean indeed takes significantly positive (though small) values

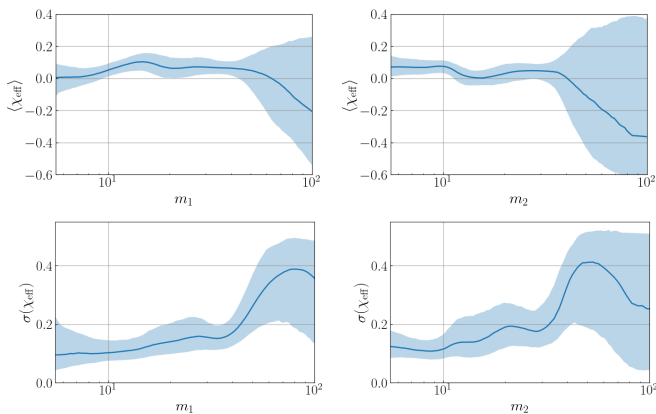


FIG. 8. The mean (top panels) and standard deviation (bottom panels) of the population  $\chi_{\text{eff}}$  distribution, as a function of primary (left) or secondary (right) mass (median and symmetric 90% confidence intervals over bootstrap iterations).

for  $m_1 \gtrsim 10 M_\odot$  and low  $m_2$ , but is generally consistent with 0 for higher mass, where statistical uncertainty grows rapidly. On the other hand the dispersion (spread) remains small at low mass and increases significantly at  $m_1 > 40 M_\odot$ , confirming findings from the parameterized analysis of [22].

#### IV. DISCUSSION

We argue that maximally flexible or data-driven methods are preferable for investigating binary black hole population properties based on GW observations, as there is currently no clear preferred astrophysical explanation of BBH formation, and restrictive assumptions may induce biases in inference. In this work we take a further step towards a general non-parametric analysis with a reconstruction of the population from GWTC-3 detections over the 3d space of component masses and effective aligned spin, arguably the parameters holding the most information on possible correlations or subpopulations (for the current set of detections confined to relatively low  $z$ ). We employ an iterative KDE-based method designed to account for finite event statistics, parameter uncertainties and selection effects [40, 43, 59].

For the BBH mass distribution, we obtain similar findings to our previous work neglecting spin effects [40], indicating features (comparable to [35]) that depart from the common assumption of a single population distribution over mass ratio.

Our reconstruction of the population over aligned spin shows bulk features similar to the LVK analyses [9, 10]: the majority of the population lies close to zero  $\chi_{\text{eff}}$ , with a preference for small positive values in regions of the mass space where the distribution is narrowly defined. Both the dispersion of the  $\chi_{\text{eff}}$  distribution and its measurement uncertainties grow noticeably for component masses above  $\sim 40 M_\odot$  (comparable to [35, 46]). Despite

such high uncertainties, we find a significant increase in the  $\chi_{\text{eff}}$  dispersion for primary mass between  $40 - 50 M_\odot$ , comparable to the transition to a broader distribution consistent with a zero mean at higher masses which is claimed in [22] to be due to hierarchical merger dominating above the expected PISN mass scale of  $\sim 45 M_\odot$ .

We partly confirm the mass ratio- $\chi_{\text{eff}}$  correlation claimed in [45, 73], as we find a positive mean  $\chi_{\text{eff}}$  above  $\sim 0.1$  only outside the near-equal-mass region inhabited by the bulk of detected events. However, this positive aligned-spin trend does not persist to high-mass asymmetric binaries; this restriction is consistent with the possibility that such correlations are due to isolated binary dynamics [e.g. 21].

We identify other trends such as an apparent positive correlation between  $\chi_{\text{eff}}$  and  $m_1$  in the low-mass BBH rate peak, possibly linked to mass transfer: overall, while these features offer hints to formation channels and guidance for astrophysical modeling, their statistical significance is not high, underscoring the need for future data to refine such interpretations. We thus expect the upcoming LVK O4 catalog releases to have a decisive role in confirming or ruling out claimed correlations and subpopulations.

Our KDE-based analysis, while flexible and computationally efficient, has some limitations. The assumption of a smooth continuous kernel reduces our ability to identify “sharp” structures in the underlying distribution, if such exist, while the sheer size of the 3d parameter space requires a large number of detections to obtain useful “local” measurements. Additionally, this study focused solely on effective spins ( $\chi_{\text{eff}}$ ), leaving in-plane spin components and spin magnitudes (not to mention possible evolution over redshift [46]) as critical future extensions. As the GW catalog grows, combining our method with improved astrophysical modeling will be crucial to disentangling the complex origins of merging black holes (e.g. [74] discusses comparison of non-parametric inference with physical models).

#### ACKNOWLEDGMENTS

The authors have benefited from conversations with Fabio Antonini, Vaibhav Tiwari, Steve Fairhurst, Will Farr and others in the LVK Binary Rates & Populations group. JS also acknowledges support from the European Union’s H2020 ERC Consolidator Grant “GRavity from Astrophysical to Microscopic Scales” (GRAMS-815673) and the EU Horizon 2020 Research and Innovation Programme under the Marie Skłodowska-Curie Grant Agreement No. 101007855. TD and ALM have received financial support from Xunta de Galicia (CIGUS Network of research centers) and the European Union, and are supported by María de Maeztu grant CEX2023-001318-M funded by MICIU/AEI/10.13039/501100011033.

The authors are grateful for computational resources provided by the LIGO Laboratory and supported by



National Science Foundation Grants PHY-0757058 and PHY-0823459. This research has made use of data or software obtained from the Gravitational Wave Open Science Center (gwosc.org), a service of the LIGO Scientific Collaboration, the Virgo Collaboration, and KAGRA. This material is based upon work supported by NSF’s LIGO Laboratory which is a major facility fully funded by the National Science Foundation, as well as the Science and Technology Facilities Council (STFC) of the United Kingdom, the Max-Planck-Society (MPS), and the State of Niedersachsen/Germany for support of the construction of Advanced LIGO and construction and operation of the GEO600 detector. Additional support for Advanced LIGO was provided by the Australian Re-

search Council. Virgo is funded, through the European Gravitational Observatory (EGO), by the French Centre National de Recherche Scientifique (CNRS), the Italian Istituto Nazionale di Fisica Nucleare (INFN) and the Dutch Nikhef, with contributions by institutions from Belgium, Germany, Greece, Hungary, Ireland, Japan, Monaco, Poland, Portugal, Spain. KAGRA is supported by Ministry of Education, Culture, Sports, Science and Technology (MEXT), Japan Society for the Promotion of Science (JSPS) in Japan; National Research Foundation (NRF) and Ministry of Science and ICT (MSIT) in Korea; Academia Sinica (AS) and National Science and Technology Council (NSTC) in Taiwan.

- 
- [1] B. P. Abbott *et al.* (LIGO Scientific, Virgo), Observation of Gravitational Waves from a Binary Black Hole Merger, *Phys. Rev. Lett.* **116**, 061102 (2016), arXiv:1602.03837 [gr-qc].
  - [2] B. P. Abbott *et al.* (LIGO Scientific, Virgo), Astrophysical Implications of the Binary Black-Hole Merger GW150914, *Astrophys. J. Lett.* **818**, L22 (2016), arXiv:1602.03846 [astro-ph.HE].
  - [3] J. Aasi *et al.* (LIGO Scientific), Advanced LIGO, *Class. Quant. Grav.* **32**, 074001 (2015), arXiv:1411.4547 [gr-qc].
  - [4] F. Acernese *et al.* (VIRGO), Advanced Virgo: a second-generation interferometric gravitational wave detector, *Class. Quant. Grav.* **32**, 024001 (2015), arXiv:1408.3978 [gr-qc].
  - [5] B. P. Abbott *et al.* (LIGO Scientific, Virgo), GWTC-1: A Gravitational-Wave Transient Catalog of Compact Binary Mergers Observed by LIGO and Virgo during the First and Second Observing Runs, *Phys. Rev. X* **9**, 031040 (2019), arXiv:1811.12907 [astro-ph.HE].
  - [6] R. Abbott *et al.* (LIGO Scientific, Virgo), GWTC-2: Compact Binary Coalescences Observed by LIGO and Virgo During the First Half of the Third Observing Run, *Phys. Rev. X* **11**, 021053 (2021), arXiv:2010.14527 [gr-qc].
  - [7] R. Abbott *et al.* (LIGO Scientific, VIRGO), GWTC-2.1: Deep extended catalog of compact binary coalescences observed by LIGO and Virgo during the first half of the third observing run, *Phys. Rev. D* **109**, 022001 (2024), arXiv:2108.01045 [gr-qc].
  - [8] R. Abbott *et al.* (KAGRA, VIRGO, LIGO Scientific), GWTC-3: Compact Binary Coalescences Observed by LIGO and Virgo during the Second Part of the Third Observing Run, *Phys. Rev. X* **13**, 041039 (2023), arXiv:2111.03606 [gr-qc].
  - [9] R. Abbott *et al.* (LIGO Scientific, Virgo), Population Properties of Compact Objects from the Second LIGO-Virgo Gravitational-Wave Transient Catalog, *Astrophys. J. Lett.* **913**, L7 (2021), arXiv:2010.14533 [astro-ph.HE].
  - [10] R. Abbott *et al.* (KAGRA, VIRGO, LIGO Scientific), Population of Merging Compact Binaries Inferred Using Gravitational Waves through GWTC-3, *Phys. Rev. X* **13**, 011048 (2023), arXiv:2111.03634 [astro-ph.HE].
  - [11] S. Vitale, R. Lynch, R. Sturani, and P. Graff, Use of gravitational waves to probe the formation channels of compact binaries, *Class. Quant. Grav.* **34**, 03LT01 (2017), arXiv:1503.04307 [gr-qc].
  - [12] C. L. Rodriguez, M. Zevin, C. Pankow, V. Kalogera, and F. A. Rasio, Illuminating Black Hole Binary Formation Channels with Spins in Advanced LIGO, *Astrophys. J. Lett.* **832**, L2 (2016), arXiv:1609.05916 [astro-ph.HE].
  - [13] W. M. Farr, S. Stevenson, M. Coleman Miller, I. Mandel, B. Farr, and A. Vecchio, Distinguishing Spin-Aligned and Isotropic Black Hole Populations With Gravitational Waves, *Nature* **548**, 426 (2017), arXiv:1706.01385 [astro-ph.HE].
  - [14] B. Farr, D. E. Holz, and W. M. Farr, Using Spin to Understand the Formation of LIGO and Virgo’s Black Holes, *Astrophys. J. Lett.* **854**, L9 (2018), arXiv:1709.07896 [astro-ph.HE].
  - [15] S. S. Bavera, T. Fragos, Y. Qin, E. Zapartas, C. J. Neijssel, I. Mandel, A. Batta, S. M. Gaebel, C. Kimball, and S. Stevenson, The origin of spin in binary black holes: Predicting the distributions of the main observables of Advanced LIGO, *Astron. Astrophys.* **635**, A97 (2020), arXiv:1906.12257 [astro-ph.HE].
  - [16] M. Zevin, S. S. Bavera, C. P. L. Berry, V. Kalogera, T. Fragos, P. Marchant, C. L. Rodriguez, F. Antonini, D. E. Holz, and C. Pankow, One Channel to Rule Them All? Constraining the Origins of Binary Black Holes Using Multiple Formation Pathways, *Astrophys. J.* **910**, 152 (2021), arXiv:2011.10057 [astro-ph.HE].
  - [17] M. Zevin and S. S. Bavera, Suspicious Siblings: The Distribution of Mass and Spin across Component Black Holes in Isolated Binary Evolution, *Astrophys. J.* **933**, 86 (2022), arXiv:2203.02515 [astro-ph.HE].
  - [18] F. S. Broekgaarden, S. Stevenson, and E. Thrane, Signatures of Mass Ratio Reversal in Gravitational Waves from Merging Binary Black Holes, *Astrophys. J.* **938**, 45 (2022), arXiv:2205.01693 [astro-ph.HE].
  - [19] J. Fuller and W. Lu, The spins of compact objects born from helium stars in binary systems, *Mon. Not. Roy. Astron. Soc.* **511**, 3951 (2022), arXiv:2201.08407 [astro-ph.HE].
  - [20] E. Payne, K. Kremer, and M. Zevin, Spin Doctors: How to Diagnose a Hierarchical Merger Origin, *Astrophys. J. Lett.* **966**, L16 (2024), arXiv:2402.15066 [gr-qc].
  - [21] S. Banerjee and A. Olejak, On the effective spin-mass ratio  $\chi_{\text{eff}} - q$  relation of binary black hole mergers that

- evolved in isolation, (2024), arXiv:2411.15112 [astro-ph.HE].
- [22] F. Antonini, I. M. Romero-Shaw, and T. Callister, Star Cluster Population of High Mass Black Hole Mergers in Gravitational Wave Data, *Phys. Rev. Lett.* **134**, 011401 (2025), arXiv:2406.19044 [astro-ph.HE].
- [23] J. Fuller and L. Ma, Most Black Holes are Born Very Slowly Rotating, *Astrophys. J. Lett.* **881**, L1 (2019), arXiv:1907.03714 [astro-ph.SR].
- [24] C. Cutler and E. E. Flanagan, Gravitational waves from merging compact binaries: How accurately can one extract the binary's parameters from the inspiral wave form?, *Phys. Rev. D* **49**, 2658 (1994), arXiv:gr-qc/9402014.
- [25] E. Baird, S. Fairhurst, M. Hannam, and P. Murphy, Degeneracy between mass and spin in black-hole-binary waveforms, *Phys. Rev. D* **87**, 024035 (2013), arXiv:1211.0546 [gr-qc].
- [26] K. K. Y. Ng, S. Vitale, A. Zimmerman, K. Chatziioannou, D. Gerosa, and C.-J. Haster, Gravitational-wave astrophysics with effective-spin measurements: asymmetries and selection biases, *Phys. Rev. D* **98**, 083007 (2018), arXiv:1805.03046 [gr-qc].
- [27] A. Q. Cheng, M. Zevin, and S. Vitale, What You Don't Know Can Hurt You: Use and Abuse of Astrophysical Models in Gravitational-wave Population Analyses, *Astrophys. J.* **955**, 127 (2023), arXiv:2307.03129 [astro-ph.HE].
- [28] L. A. C. van Son, S. E. de Mink, T. Callister, S. Justham, M. Renzo, T. Wagg, F. S. Broekgaarden, F. Kummer, R. Pakmor, and I. Mandel, The Redshift Evolution of the Binary Black Hole Merger Rate: A Weighty Matter, *Astrophys. J.* **931**, 17 (2022), arXiv:2110.01634 [astro-ph.HE].
- [29] S. S. Bavera, M. Fishbach, M. Zevin, E. Zapartas, and T. Fragos, The  $\chi_{\text{eff}} - z$  correlation of field binary black hole mergers and how 3G gravitational-wave detectors can constrain it, *Astron. Astrophys.* **665**, A59 (2022), arXiv:2204.02619 [astro-ph.HE].
- [30] I. Mandel, Parameter estimation on gravitational waves from multiple coalescing binaries, *Phys. Rev. D* **81**, 084029 (2010), arXiv:0912.5531 [astro-ph.HE].
- [31] E. Thrane and C. Talbot, An introduction to Bayesian inference in gravitational-wave astronomy: parameter estimation, model selection, and hierarchical models, *Publ. Astron. Soc. Austral.* **36**, e010 (2019), [Erratum: *Publ. Astron. Soc. Austral.* **37**, e036 (2020)], arXiv:1809.02293 [astro-ph.IM].
- [32] J. Powell, S. Stevenson, I. Mandel, and P. Tino, Unmodelled Clustering Methods for Gravitational Wave Populations of Compact Binary Mergers, *Mon. Not. Roy. Astron. Soc.* **488**, 3810 (2019), arXiv:1905.04825 [astro-ph.HE].
- [33] V. Tiwari and S. Fairhurst, The Emergence of Structure in the Binary Black Hole Mass Distribution, *Astrophys. J. Lett.* **913**, L19 (2021), arXiv:2011.04502 [astro-ph.HE].
- [34] V. Tiwari, VAMANA: modeling binary black hole population with minimal assumptions, *Class. Quant. Grav.* **38**, 155007 (2021), arXiv:2006.15047 [astro-ph.HE].
- [35] V. Tiwari, Exploring Features in the Binary Black Hole Population, *Astrophys. J.* **928**, 155 (2022), arXiv:2111.13991 [astro-ph.HE].
- [36] S. Rinaldi and W. Del Pozzo, (H)DPGMM: a hierarchy of Dirichlet process Gaussian mixture models for the inference of the black hole mass function, *Mon. Not. Roy. Astron. Soc.* **509**, 5454 (2021), arXiv:2109.05960 [astro-ph.IM].
- [37] J. Sadiq, T. Dent, and D. Wysocki, Flexible and fast estimation of binary merger population distributions with an adaptive kernel density estimator, *Phys. Rev. D* **105**, 123014 (2022), arXiv:2112.12659 [gr-qc].
- [38] B. Edelman, B. Farr, and Z. Doctor, Cover Your Basis: Comprehensive Data-driven Characterization of the Binary Black Hole Population, *Astrophys. J.* **946**, 16 (2023), arXiv:2210.12834 [astro-ph.HE].
- [39] T. A. Callister and W. M. Farr, Parameter-Free Tour of the Binary Black Hole Population, *Phys. Rev. X* **14**, 021005 (2024), arXiv:2302.07289 [astro-ph.HE].
- [40] J. Sadiq, T. Dent, and M. Gieles, Binary Vision: The Mass Distribution of Merging Binary Black Holes via Iterative Density Estimation, *Astrophys. J.* **960**, 65 (2024), arXiv:2307.12092 [astro-ph.HE].
- [41] A. Toubiana, M. L. Katz, and J. R. Gair, Is there an excess of black holes around 20  $M_{\odot}$ ? Optimizing the complexity of population models with the use of reversible jump MCMC., *Mon. Not. Roy. Astron. Soc.* **524**, 5844 (2023), arXiv:2305.08909 [gr-qc].
- [42] J. Heinzel, M. Mould, S. Álvarez-López, and S. Vitale, High resolution nonparametric inference of gravitational-wave populations in multiple dimensions, *Phys. Rev. D* **111**, 063043 (2025), arXiv:2406.16813 [astro-ph.HE].
- [43] J. Sadiq, T. Dent, and A. L. Medina, Looking to the horizon: Probing evolution in the black hole spectrum with gw catalogs, (2025), arXiv:2502.06451 [gr-qc].
- [44] P. Ajith *et al.*, Inspiral-merger-ringdown waveforms for black-hole binaries with non-precessing spins, *Phys. Rev. Lett.* **106**, 241101 (2011), arXiv:0909.2867 [gr-qc].
- [45] T. A. Callister, C.-J. Haster, K. K. Y. Ng, S. Vitale, and W. M. Farr, Who Ordered That? Unequal-mass Binary Black Hole Mergers Have Larger Effective Spins, *Astrophys. J. Lett.* **922**, L5 (2021), arXiv:2106.00521 [astro-ph.HE].
- [46] S. Biscoveanu, T. A. Callister, C.-J. Haster, K. K. Y. Ng, S. Vitale, and W. M. Farr, The Binary Black Hole Spin Distribution Likely Broadens with Redshift, *Astrophys. J. Lett.* **932**, L19 (2022), arXiv:2204.01578 [astro-ph.HE].
- [47] M. Fishbach, D. E. Holz, and W. M. Farr, Does the Black Hole Merger Rate Evolve with Redshift?, *Astrophys. J. Lett.* **863**, L41 (2018), arXiv:1805.10270 [astro-ph.HE].
- [48] A. Lorenzo-Medina and T. Dent, A physically modelled selection function for compact binary mergers in the LIGO-Virgo O3 run and beyond, *Class. Quant. Grav.* **42**, 045008 (2025), arXiv:2408.13383 [gr-qc].
- [49] G. Franciolini and P. Pani, Searching for mass-spin correlations in the population of gravitational-wave events: The GWTC-3 case study, *Phys. Rev. D* **105**, 123024 (2022), arXiv:2201.13098 [astro-ph.HE].
- [50] V. Baibhav, Z. Doctor, and V. Kalogera, Dropping Anchor: Understanding the Populations of Binary Black Holes with Random and Aligned-spin Orientations, *Astrophys. J.* **946**, 50 (2023), arXiv:2212.12113 [astro-ph.HE].
- [51] J. Godfrey, B. Edelman, and B. Farr, Cosmic cousins: Identification of a subpopulation of binary black holes consistent with isolated binary evolution, (2024), arXiv:2304.01288 [astro-ph.HE].
- [52] A. Ray, I. M. Hernandez, K. Breivik, and J. Creighton,

- Searching for binary black hole sub-populations in gravitational wave data using binned gaussian processes, (2024), arXiv:2404.03166 [astro-ph.HE].
- [53] F. Antonini, M. Gieles, F. Dosopoulou, and D. Chattopadhyay, Coalescing black hole binaries from globular clusters: mass distributions and comparison to gravitational wave data from GWTC-3, *Mon. Not. Roy. Astron. Soc.* **522**, 466 (2023), arXiv:2208.01081 [astro-ph.HE].
  - [54] Y.-J. Li, Y.-Z. Wang, S.-P. Tang, and Y.-Z. Fan, Resolving the Stellar-Collapse and Hierarchical-Merger Origins of the Coalescing Black Holes, *Phys. Rev. Lett.* **133**, 051401 (2024), arXiv:2303.02973 [astro-ph.HE].
  - [55] Y.-J. Li, S.-P. Tang, S.-J. Gao, D.-C. Wu, and Y.-Z. Wang, Exploring Field-evolution and Dynamical-capture Coalescing Binary Black Holes in GWTC-3, *Astrophys. J.* **977**, 67 (2024), arXiv:2404.09668 [astro-ph.HE].
  - [56] G. Pierra, S. Mastrogiovanni, and S. Perriès, The spin magnitude of stellar-mass black holes evolves with the mass, *Astron. Astrophys.* **692**, A80 (2024), arXiv:2406.01679 [gr-qc].
  - [57] J. Heinzl, M. Mould, and S. Vitale, Nonparametric analysis of correlations in the binary black hole population with LIGO-Virgo-KAGRA data, *Phys. Rev. D* **111**, L061305 (2025), arXiv:2406.16844 [astro-ph.HE].
  - [58] LIGO Scientific, Virgo and KAGRA Collaborations, GWTC-3: Parameter estimation data release (2021).
  - [59] J. Sadiq, K. Dey, T. Dent, and E. Barausse, Reconstructing the LISA massive black hole binary population via iterative kernel density estimation, *Phys. Rev. D* **111**, 063051 (2025), arXiv:2410.17056 [gr-qc].
  - [60] B. Silverman, *Density Estimation for Statistics and Data Analysis*, 1st ed. (Chapman and Hall, London, 1986).
  - [61] E. Payne and E. Thrane, Model exploration in gravitational-wave astronomy with the maximum population likelihood, *Phys. Rev. Res.* **5**, 023013 (2023), arXiv:2210.11641 [astro-ph.IM].
  - [62] LIGO Scientific, Virgo and KAGRA Collaborations, GWTC-3: O1+O2+O3 Search Sensitivity Estimates (2021).
  - [63] LIGO Scientific, Virgo and KAGRA Collaborations, Gwtc-3: O3 search sensitivity estimates (2023).
  - [64] J. Veitch *et al.*, Parameter estimation for compact binaries with ground-based gravitational-wave observations using the LALInference software library, *Phys. Rev. D* **91**, 042003 (2015), arXiv:1409.7215 [gr-qc].
  - [65] T. A. Callister, A thesaurus for common priors in gravitational-wave astronomy, (2021), arXiv:2104.09508 [gr-qc].
  - [66] R. Abbott *et al.* (LIGO Scientific, Virgo), GW190814: Gravitational Waves from the Coalescence of a 23 Solar Mass Black Hole with a 2.6 Solar Mass Compact Object, *Astrophys. J. Lett.* **896**, L44 (2020), arXiv:2006.12611 [astro-ph.HE].
  - [67] V. Baibhav, D. Gerosa, E. Berti, K. W. K. Wong, T. Helfer, and M. Mould, The mass gap, the spin gap, and the origin of merging binary black holes, *Phys. Rev. D* **102**, 043002 (2020), arXiv:2004.00650 [astro-ph.HE].
  - [68] S. E. Woosley and A. Heger, The Pair-Instability Mass Gap for Black Holes, *Astrophys. J. Lett.* **912**, L31 (2021), arXiv:2103.07933 [astro-ph.SR].
  - [69] M. Mould, D. Gerosa, F. S. Broekgaarden, and N. Steinle, Which black hole formed first? Mass-ratio reversal in massive binary stars from gravitational-wave data, *Mon. Not. Roy. Astron. Soc.* **517**, 2738 (2022), arXiv:2205.12329 [astro-ph.HE].
  - [70] A. Olejak, J. Klencki, X.-T. Xu, C. Wang, K. Belczynski, and J.-P. Lasota, Unequal-mass, highly-spinning binary black hole mergers in the stable mass transfer formation channel, *Astron. Astrophys.* **689**, A305 (2024), arXiv:2404.12426 [astro-ph.HE].
  - [71] L. A. C. van Son, S. E. de Mink, M. Renzo, S. Justham, E. Zapartas, K. Breivik, T. Callister, W. M. Farr, and C. Conroy, No Peaks without Valleys: The Stable Mass Transfer Channel for Gravitational-wave Sources in Light of the Neutron Star-Black Hole Mass Gap, *Astrophys. J.* **940**, 184 (2022), arXiv:2209.13609 [astro-ph.HE].
  - [72] S. Galadage and A. Lamberts, Compactness peaks: An astrophysical interpretation of the mass distribution of merging binary black holes, *Astron. Astrophys.* **694**, A186 (2025), arXiv:2407.17561 [astro-ph.HE].
  - [73] C. Adamcewicz, P. D. Lasky, and E. Thrane, Evidence for a Correlation between Binary Black Hole Mass Ratio and Black Hole Spins, *Astrophys. J.* **958**, 13 (2023), arXiv:2307.15278 [astro-ph.HE].
  - [74] C. M. Fabbri, D. Gerosa, A. Santini, M. Mould, A. Toubiana, and J. Gair, Reconstructing parametric gravitational-wave population fits from non-parametric results without refitting the data, (2025), arXiv:2501.17233 [astro-ph.HE].